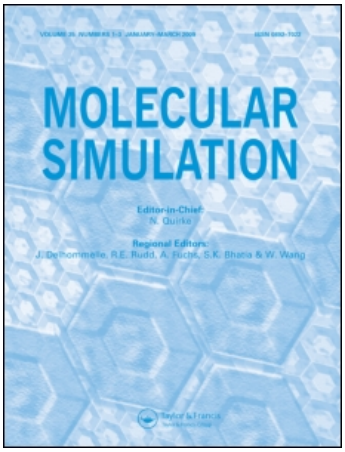

Molecular Simulation
Publication details, including instructions for authors and subscription information:
http://www.informaworld.com/smpp/title~content=t713644482

Molecular Modelling of the Mechanism of Action of Borate Retarders on Hydrating Cements at High Temperature

I. S. Bell[ab]; P. V. Coveney[a]
[a] Schlumberger Cambridge Research, Cambridge, United Kingdom [b] Department of Chemistry, University of Cambridge, Cambridge, United Kingdom

To cite this Article Bell, I. S. and Coveney, P. V.(1998) 'Molecular Modelling of the Mechanism of Action of Borate Retarders on Hydrating Cements at High Temperature', Molecular Simulation, 20: 6, 331 — 356
To link to this Article: DOI: 10.1080/08927029808022042
URL: http://dx.doi.org/10.1080/08927029808022042

Molecular Simulation, 1998, Vol. 20, pp. 331–356
Reprints available directly from the publisher
Photocopying permitted by license only

MOLECULAR MODELLING OF THE MECHANISM OF ACTION OF BORATE RETARDERS ON HYDRATING CEMENTS AT HIGH TEMPERATURE

I. S. BELL * and P. V. COVENEY †

Schlumberger Cambridge Research, High Cross, Madingley Road, Cambridge CB3 0HG, United Kingdom

(Received August 1997; accepted September 1997)

We consider the class of borate additives in an attempt to understand, on the basis of molecular modelling techniques, why they are effective high temperature cement setting retarder aids. Borates are known to act as cement retarders under ambient conditions, for which the Billingham-Coveney clock reaction scheme[1] based on a gel → crystalline ettringite transformation provides the basic model. Under conditions of high temperature (above ca. 80°C) ettringite is known to be unstable, so that a modification to this mechanism is then required. However, conceptually (and mathematically) the kinetic scheme remains unchanged: we are concerned with a gel → crystalline silicate transition, which can be inhibited by suitable retarders. Thus the proposed mechanism for the high temperature retardation of hydrating cements by borates is that the latter prevent the growth of polymeric or crystalline calcium silicate hydrates such as tobermorite from the initially formed C—S—H gel.

The mechanism which we propose in this paper, which is based on chemisorption of borate species, explains some experimentally observed phenomena relating to the retarding action of both monomeric and polymeric borates in solution. On the basis of this work, we are able to predict vibrational frequencies for the cyclic borosilicate species which is formed, observation of which would confirm the validity of the mechanism proposed here. We can also use our work to explain the effectiveness of different borates. We conclude by suggesting a novel boronate retarder which might be expected to be more potent than those currently in use.

Keywords: Borate retarder; cement slurries; Billingham-Coveney scheme; nucleation and crystal growth

* Present address: Department of Chemistry, University of Cambridge, Lensfield Road, Cambridge CB2 1EW, United Kingdom.
† Author to whom correspondence should be addressed.

1. INTRODUCTION

In oil well cementing, a cement slurry is pumped down the steel casing of the well and up the annular space between it and the surrounding rock. The main objectives are to restrict movement of fluids between formations at different levels and to support and protect the casing. The slurry must remain sufficiently fluid for the pumping operation to be completed and to this end cement setting retarders are widely employed, especially in deeper wells.

Existing understanding of the mechanism of action of cement retarders is thin (cf. Taylor's book [2]); however phosphonate compounds have long been recognised as efficient retarders for well cements at ambient temperatures. A previous molecular modelling study by Coveney and Humphries has provided a mechanism by which phosphonates may inhibit the nucleation and subsequent growth of crystalline ettringite from its gelatinous precursor, thereby retarding setting of the cement slurry [3]. The proposed mechanism has been confirmed by experimental studies, including some reported in that paper [3] as well as more detailed work which has subsequently been carried out [4].

The temperature at the bottom of a deep oil well (which can reach a depth of up to 6000 m) is 100–250°C, and the pressure experienced by the slurry during pumping may be as much as 150 MPa. Under such extreme conditions, the effectiveness of phosphonate retarders is reduced and other compounds must be added to the slurry in order to slow its setting. Borates, particularly borax ($Na_2B_4O_7 \cdot 10H_2O$), have been used regularly in oilwell cementing operations both as conventional retarders and also as high-temperature retarder aids. Under ambient conditions, borates retard slurries by the same mechanism as phosphonates, although not as effectively, as described in [3], incorporation of $B(OH)_4^-$ or HBO_3^{2-} units in place of sulphate groups in the crystal lattice of ettringite inhibiting its nucleation and growth.

It is known that ettringite is unstable above about 80°C, presumably decomposing to give the crystalline "monosulphate", so that this mechanism can only be partially valid at high temperature. Note, however, that phosphonates are still essential to the overall retardation so we can reasonably assume that a similar mechanism is still involved, albeit less centrally than at low temperature.

The principal reaction leading to the setting of cement is

$$C_3S + nH_2O \rightarrow CSH + CH, \tag{1}$$

where C_3S denotes tricalcium silicate, generally present as a mass fraction of 50–70% of the cement grains, CH represents calcium hydroxide

(portlandite) and CSH is hydrated calcium silicate gel. It is this gel which is responsible for the strength and dimensional stability of the set cement at ordinary temperatures. Monomeric and oligomeric (mainly dimeric) CSH are also the early hydration products at elevated temperature and pressure [2]. (Here and throughout we shall use cement chemical notation to denote many of the chemical species, with compounds being expressed as a sum of oxides. For example tricalcium silicate, Ca_3SiO_5, can be written as $3CaO{\cdot}SiO_2$. Abbreviations are then given to the oxides frequently encountered such as C for CaO, S for SiO_2 and H for H_2O. Thus Ca_3SiO_5 becomes C_3S. See Ref. [2] for further elaboration.)

Although CSH gel is practically amorphous in that it has no long-range order, various studies have indicated short-range structural relationships to the naturally occurring minerals tobermorite and jennite. Fujii and Kondo [5] treated CSH gel as a solid solution of tobermorite and CH, while Kantro *et al.* [6] proposed a model in which tobermorite layers are sandwiched between calcium hydroxide. Taylor's model [7] assumed the CSH gel to have a disordered layer structure, consisting of structurally imperfect layers of tobermorite and jennite. In each of these cases, the CSH gel is modelled as consisting of short-range ordered crystalline phases of calcium silicate hydrates with no overall long-range order.

The approach which we have taken in this paper is to assume that by impeding the growth of both polymeric silicate chains and crystalline calcium silicate hydrate phases such as tobermorite from monomeric CSH, we will retard the setting of the cement in the high temperature regime. We model this process

$$\text{CSH} \rightarrow \text{polymeric silicate} \tag{2}$$

by an inhibited autocatalytic nucleation mechanism. There is evidence of the plausibility of this approach: Casey *et al.*, gave direct evidence of "gel"-like material in hydrating chain-silicate materials due to leaching by H_2O [8]. Note that the polymeric species specified by (2) may be either crystalline or gelatinous in nature.

Using the modelling approach of the Billingham-Coveney clock model [1, 3] as a basis, we focus on what we believe to be the rate-determining steps in the overall hydration process. We make the following choice of labels for the species occurring in that model:

$$\begin{aligned} \text{P} &= \text{C}_3\text{S}, \\ \text{A} &= \text{monomeric CSH}, \end{aligned} \tag{3}$$

B = polymeric silicate,
C = inhibitor such as borate,
D = poisoned species.

and allow for CSH to react via inhibited autocatalysis. We then arrive at the kinetic scheme

$$\begin{aligned} \mathrm{P} &\rightarrow \mathrm{A}, \quad \text{rate} = k_0 p, \\ \mathrm{A} &\rightarrow \mathrm{B}, \quad \text{rate} = k_1 a, \\ \mathrm{A} + 2\mathrm{B} &\rightarrow 3\mathrm{B}, \quad \text{rate} = k_2 a b^2, \\ \mathrm{B} + \mathrm{C} &\rightarrow \mathrm{D}, \quad \text{rate} = k_3 b^m c. \end{aligned} \tag{4}$$

Note that kinetic schemes such as these are manifestly of a *macroscopic* nature: all the individual growth processes such as polymerisation and nucleation have been subsumed within this coarse-grained description. In recent work, Wattis and Coveney [9] have shown how these macroscopic descriptions emerge from a contraction of the full microscopic kinetics.

In the scheme above, B may be any polymeric (including crystalline) calcium silicate hydrate; C is the borate retarder. The reason for the choice of stoichiometric coefficients in the second step has been discussed previously [1, 3]. This is likely to be only a crude approximation [9], but such details are not important in the current work. At 110°C, the stable crystalline product of the conversion from CSH is tobermorite ($C_5S_6H_5$); the high strength and low permeability of the gel are preserved. As the curing temperature increases to 150°C, tobermorite normally converts to xonotlite (C_6S_6H) with minimal deterioration. However, it has been reported that tobermorite can sometimes persist up to 250°C in Portland cement systems because of aluminium substitution in the lattice structure [10]. Above 400°C, xonotlite dehydrates, resulting in the disintegration of the set cement. The phase jennite is only stable below 100°C. These phases (and several more) have similar structures comprising long silicate chains. Our main argument is that such crystalline phases, as well as amorphous polymeric silicates, undergo the same mechanism of growth inhibition by borates.

Indeed, the inhibition of the growth of hydrated silicate chains provides the central element about which our molecular modelling work is based. In Section 2, the structure and morphology of tobermorite is analysed in detail in order to determine the mechanism of crystal growth; xonotlite is also considered here. Section 3 deals with the molecular and chemical properties of borates, and Section 4 provides a mechanism by which such ions may slow the growth of tobermorite crystals. We then go on to predict some

experimental data which could be observed in the future and which would substantiate the mechanism proposed here. On the basis of this work we can rationalise the effectiveness of borate retarders, and in Section 5 we are able to propose a novel boronate retarder that we might expect to be more effective than those used at present. The paper ends with some general conclusions from the present work. The appendices contain further data on the spectroscopic calculations we make.

2. CRYSTAL STRUCTURE AND MORPHOLOGY OF TOBERMORITE

As described above, the growth of polymeric silicate chain species in the cement slurry is a key step in controlling the high temperature setting process. It is therefore necessary to consider in detail the structure of such chains. We take tobermorite as a representative example in order to determine a possible mechanism for growth inhibition by borate retarders.

The crystal structure of a natural tobermorite from Zeilberg, Maroldsweisach, Germany was solved by Hamid using X-ray diffraction data [11]. Hamid went on to propose an ordered structure with a monoclinic cell of space group $P2_1$, unique axis c, and lattice constants $a = 6.69$ Å, $b = 7.39$ Å, $c = 22.77$ Å and $\gamma = 123.49°$. The atomic co-ordinates are also given for this ordered structure, and it was these which were used to build the crystal lattice [12].

The tobermorite structure consists of infinite chains of $Si_3(O/OH)_9$ tetrahedra running parallel to b which are linked together by calcium atoms (Fig. 1). The mean Si —O distance is 1.62 Å and the average value of the O —O distances in the $Si_3(O/OH)_9$ chains is 2.64 Å. Each of the calcium atoms is co-ordinated by seven oxygens. The unit cell contains nine calcium atoms of which eight are in fixed positions; the ninth is statistically distributed amongst four positions in the cell. The average Ca —O distance is 2.47 Å for the fixed calciums, and 2.99 Å for the statistically distributed atom. The overall content of the monoclinic tobermorite unit cell in space group $P2_1$ is therefore $Ca_9Si_{12}O_{30}(OH)_6 \cdot 4H_2O$ which, given the cell volume of 938.84 $Å^3$, corresponds to a density of 2.391 g/cm^3.

We can obtain a guestimate of the morphology of tobermorite by using the Bravais Friedel Donnay Harker (BFDH) method. This algorithm computes the crystal morphology on the basis of the interplanar atomic spacings and the crystal symmetry [13–15]. The closer the lattice spacing, the faster the surface grows. The distance of the crystal face from the centre

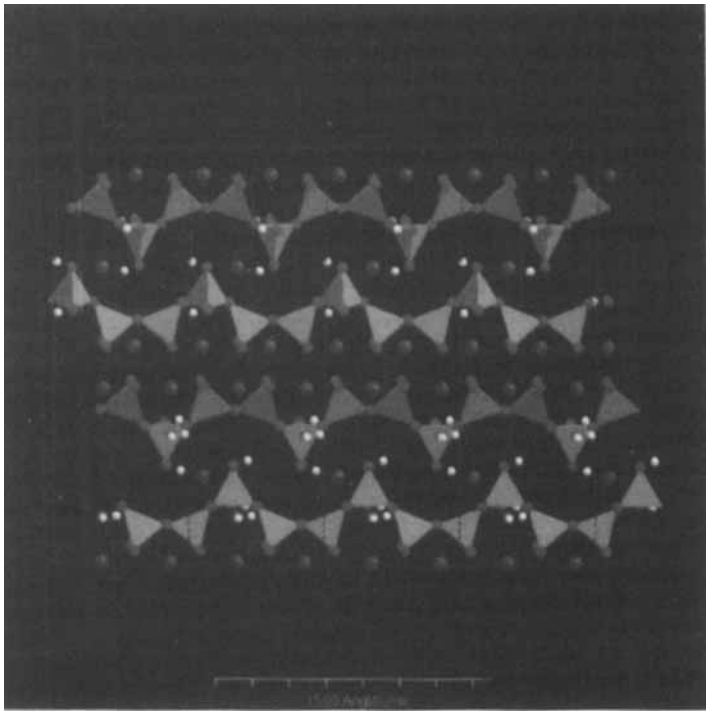

FIGURE 1 The crystal structure of tobermorite (Ca: blue, Si: orange, O: red, H: white). (See Color Plate I).

of the crystal is taken to be inversely proportional to the lattice spacing. In reality, the algorithm is a very crude approximation as it completely neglects the energetics of ion attachment, which however is more difficult to compute reliably owing to the long-range nature of the coulombic interaction. For these reasons, it is best to regard the algorithm as essentially empirical. A first order estimate of the morphology computed in this way is shown in Figure 2.

However, it is known that specimens of tobermorite crystallize as thin, pseudo-hexagonal plates with (001) cleavage and a tendency to elongation parallel to *b*. We found it possible to reproduce this observed morphology by adjusting the relative growth rates of the faces seen in Figure 2. Figure 3 shows the resulting morphology, which closely resembles that found experimentally. The observation that the crystal grows fastest parallel to *b* is important in what follows, for the effectiveness of crystal nucleation and growth inhibitors is largely controlled by their interaction with the fastest growthing surfaces. Since the silicate chains in tobermorite propagate in the

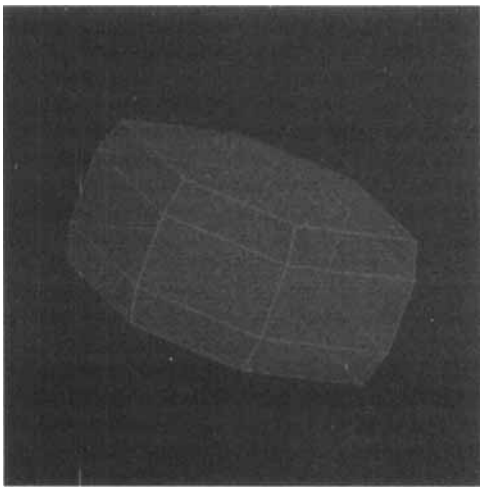

FIGURE 2 First order estimate of tobermorite morphology. (See Color Plate II).

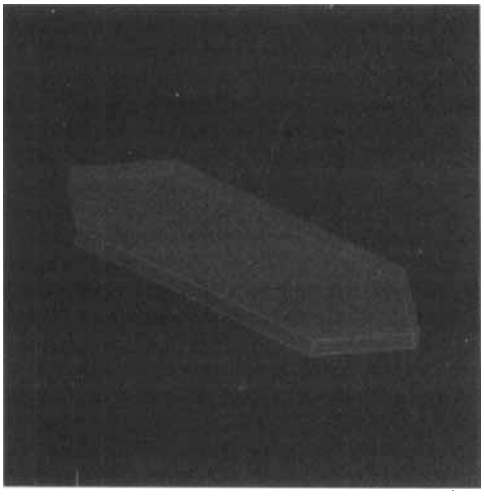

FIGURE 3 The observed tobermorite crystal morphology obtained by adjusting the relative growth rates of the crystal surfaces. (See Color Plate III).

b direction, it is apparent that this fastest growing surface has the chains of SiO_4 tetrahedra running orthogonally to it. It therefore seems likely that the mechanism of action of borte retarders is related to their ability to prevent the extension of the silicate chains in the *b* direction.

At temperatures greater than 150°C, the stable silicate phase under well conditions is not tobermorite but xonotlite (C_6S_6H), although thermodynamic equilibrium is not achieved rapidly [10]. The structure of this

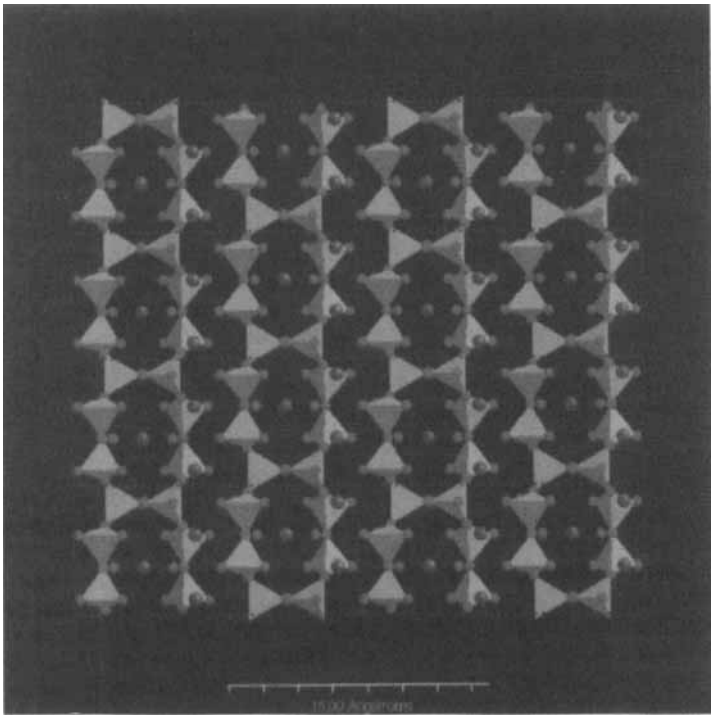

FIGURE 4 The crystal structure of xonotlite. (See Color Plate IV).

mineral is shown in Figure 4. It consists of infinite chains of rings of silicates, again propagating in the *b* direction, with each ring consisting of eight SiO_4 tetrahedra. As we shall see in Section 4 when we come to consider our proposed mechanisms of retardation, however, the precise details of the structure of such silicate phases are unimportant: we need only note for now that a suitable mechanism for inhibiting growth of xonotlite is to prevent extension of the silicate-ring chains in the *b* direction. We shall however find it necessary to consider the structure again in more detail when we come to our proposal for a novel retarder in Section 5.

3. BORATE RETARDERS

Borates are currently of interest in oil well cementing since they are being used as high-temperature cement retarders in conjunction with phosphonates. Michaux found that for a given phosphonate concentration, and independent of temperature in the range 138 – 204°C, the initial setting time

of a cement slurry is always delayed by increasing the concentration of borax (sodium tetraborate decahydrate) [16]. A comparative study of the effectiveness of a range of borate retarders has been carried out by Bensted *et al.* [17]. Although performed at relatively low temperatures, it provides useful information about possible active borate species. The study found that whilst all of the borates retarded cement setting, some did so to a greater extent than others. In order to explain this, one must consider the chemistry of borates in aqueous solution [18].

In the crystalline state, linear and cyclic borate polyanions exist with BO_3 and BO_4 units being linked by shared oxygens. However, some degree of depolymerisation of these polyanions rapidly occurs on dilution with water; such depolymerisation is especially favoured in dilute solutions of strong acidity or basicity (see [17] and references therein). Figure 5 shows the species occurring in solution as the pH is increased. The triborate species (**B**), for example, is stable from pH 8 to 10 at concentrations above 0.025 M.

NMR and pH titration studies have shown that polyborate ions such as $B_5O_{10}^{5-}$ (**A**) can exist in solution. In the work of Bensted *et al.*, however, low concentrations (< 0.02 M) and high basicity were used and so the equilibrium may be expected to lie almost entirely over to the $B(OH)_4^-$ monomeric form. This study found a fairly good correlation between the maximum amount of monomer which each borate may release and its retarding ability, as shown in Table I.

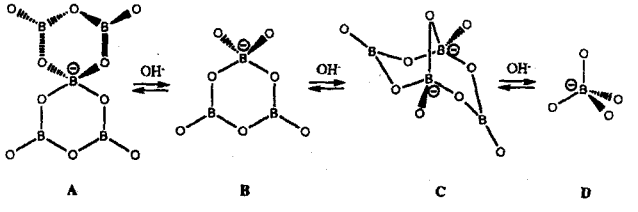

FIGURE 5 Borate species occurring in solution as a function of pH (hydrogen atoms have been omitted).

TABLE I Maximum monomer release and degree of retardation for different borates, normalized with respect to sodium tetraborate

Borate	*Maximum monomer concentration*	*Degree of Retardation*	
		22°C	*52°C*
Sodium tetraborate	1.00	1.0	1.0
Potassium tetraborate	1.22	1.1	1.1
Ammonium biborate	1.44	1.3	1.3
Disodium octaborate	1.83	1.5	1.4
Sodium pentaborate	1.61	1.4	1.3
Potassium pentaborate	1.61	1.3	1.2
Ammonium pentaborate	1.74	1.3	1.2

Any proposed mechanism of retardation must therefore enable both the monomeric form (as present under the conditions used by Bensted *et al.*, and which is likely to be the predominant form at high temperature) and the polymeric forms (as would be present at lower basicity or higher concentration as in the work of Michaux [16]) of the borates to prevent the growth of the silicate chains, as our model does. In addition to the monomeric $B(OH)_4^-$ anion, we also chose to study the pentaborate anion shown in Figure 6 as a representative polymeric species. Sodium pentaborate answers well to the requirements necessary for a reliable high-temperature retarder: good retardation and a liquid version of borate (its solubility is 15.4% by weight of saturated solution at 25°C). The modelling approach which we have adopted requires that the molecular structure of this species be considered in detail before analysing its interaction with the growing silicate chains.

MOPAC [19] was used (with calculations performed at the MNDO level) to determine the ground state of the pentaborate anion, $B_5O_{10}^{5-}$, in its fully charged (−5) state; this is shown in Figure 6. The structure consists of two six-atom boroxine (B_3O_3) rings joined at a single boron atom, with four oxygen atoms attached to the rings. Four of the B atoms in this anion have trigonal planar (sp^2) co-ordination, whilst the central B atom has tetrahedral (sp^3) geometry. The structure is stabilised by $O(2p) \rightarrow B(2p)$ π-bonding with the p_z orbital on each of the sp^2 B atoms acting as an acceptor orbital. Evidence for this bonding scheme is provided by considering the bond-

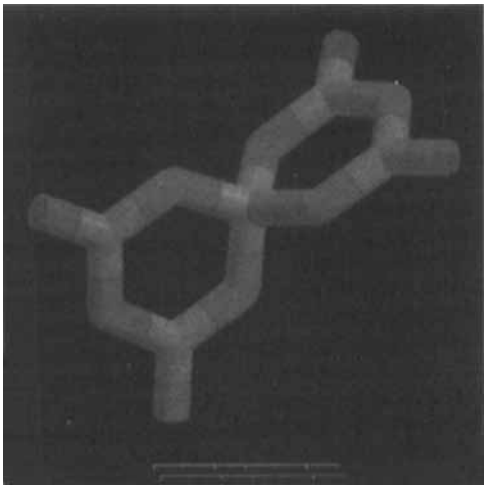

FIGURE 6 Energy minimised conformation of the pentaborate anion (B: green, O: red). (See Color Plate V).

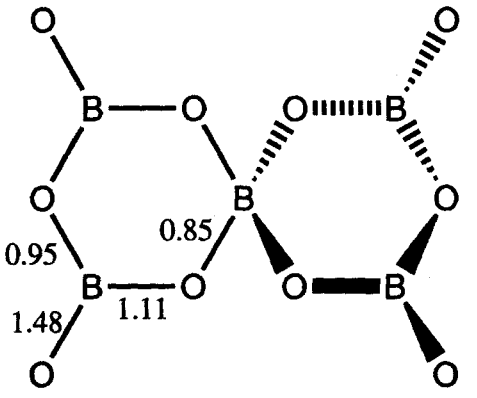

FIGURE 7 Boron-oxygen bond orders in the pentaborate anion.

orders between the various B —O pairs as calculated by MOPAC (Fig. 7), which indicates that the B —O bonds are stronger in the case of the sp^2 B atoms due to their additional π-bonding interactions. The B —O bond lengths are also indicative of the degree of π-bonding, and follow closely the pattern of the bond-orders (greater bond-order giving a shorter bond).

4. PROPOSED MECHANISM OF RETARDATION

The study of the morphology of tobermorite crystals in Section 2 confirms that the borate retarders most likely inhibit nucleation and subsequent growth of the crystals along the direction of propagation of the silicate chains, *b*, if they are to be most effective. Two channels of investigation are now considered:

(i) that the borate ions may physically adsorb to a surface perpendicular to the silicate chains in such a way so as to block further growth along a chain;
(ii) that the borate ions bond chemically to the silicate at the end of a chain thus blocking its continued propagation.

4.1. Physisorption of Borates to the Crystal Surface

Given the cell parameters $\alpha = 90°$, $\beta = 90°$ and $\gamma = 123.49°$, the surface perpendicular to the *b* direction is the $(\bar{1}20)$ plane. This surface is shown in Figure 8. The energetics of the interaction between the borate ions and this

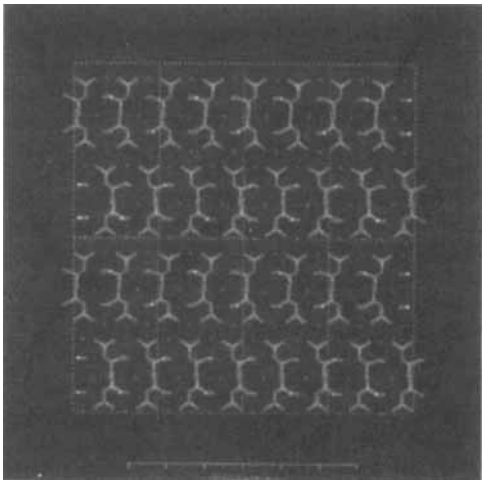

FIGURE 8 The ($\bar{1}20$) surface of tobermorite. (See Color Plate VI).

surface were then considered at the force field level. Each MOPAC-generated borate is positioned in turn at what is considered a reasonable starting site above the crystal surface, and the minimization procedure is performed. We used the so-called Universal Force Field [20], which as its name suggests is an all-purpose albeit approximate force field for general molecular and crystal structures. We included hydrogen-bonding terms, and used a distance-dependent dielectric 'constant' $\varepsilon_r r$ (ε_r being the relative permittivity and r the distance, ε_r set at 1.0) to represent the effect of the aqueous medium. The molecule's atoms were movable and the ions of the crystalline structure fixed in place [3]. To handle the long range coulomb interactions a cubic spline function was used which comes into effect at a distance of 8.0 Å and enforces a cut-off at 8.5 Å. A non-bond list with a cut-off of 9.0 Å was used. Charge equilibration was performed using the Qeq technique [21].

Molecular dynamics was then performed on the surface-plus-molecule system using an adiabatic technique [22, 23] for 50,000 steps each of 0.001 ps (= 1 fs) duration, with the atoms in the crystal lattice again fixed. The purpose of this was to avoid trapping in local minima during the minimisation. The final conformation obtained is that which has the minimum potential energy found during execution. Figure 9 shows the result of energy minimisation followed by molecular dynamics for the pentaborate ion on the ($\bar{1}20$) surface of tobermorite.

From this figure, it may be seen that the dominant effect in determining the conformation adopted by the pentaborte ion is the electrostatic

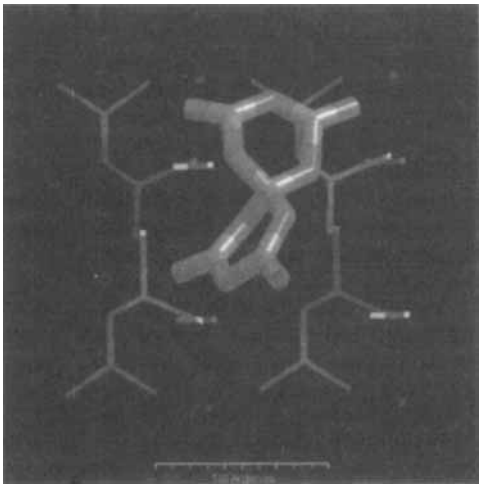

FIGURE 9 The result of energy minimisation followed by molecular dynamics for the pentaborate ion on this surface. (See Color Plate VII).

attraction between Ca^{2+} ions at the crystal surface, and the oxygen atoms on the borate anion. The MOPAC calculation performed on the pentaborate gave the charges on the external oxygens as −0.77 electronic units, and those oxygens within the boroxine rings averaged −0.36. The calcium atoms were able to complete their co-ordination of oxygens in this manner, the Ca—O distances being 2.39Å, 2.42Å and 3.06Å, comparable with the Ca—O bond lengths within the crystal. The geometrical conformation adopted by the remainder of the pentaborate anion in this case, however, does not provide a mechanism for inhibiting the growth of the silicate chains. In addition, this form of adsorption to the crystal surface cannot explain why the monomeric borate anion, $B(OH)_4^-$, is able to block growth of the chains since it would be expected to adsorb almost exclusively near to the surface calcium ions (the most electrostatically favourable sites) rather than near the surface silicates.

4.2. Chemisorption of Borates to the Silicate Chains

The "obvious" method of attaching the pentaborate anion to the silicate group at the end of a chain is by linking the silicate to one of the sp^2 boron atoms *via* a bridging oxygen atom, as shown in Figure 13(a). However, any attempt to optimise the conformation of this structure using MOPAC resulted in failure to achieve a self-consistent molecular orbital calculation. This was probably because of the large amount of negative charge in the

vicinity of the silicon atom causing instability of the structure. The same problem resulted when an attempt was made to minimise a structure comprising a monomeric $B(OH)_4^-$ unit linked to an SiO_4 tetrahedron by a single bridging oxygen atom.

The only other method of bonding the pentaborate anion to the silicate in this way is to form a four-membered ring containing the silicon atom, two bridging oxygen atoms and one of the sp^2 boron atoms (this boron atom thus becoming sp^3 hybridized), as shown in Figure 13(b). The optimised conformation of this structure as calculated by MOPAC is shown in Figure 10. The ring is virtually planar; the Si—O distance is 1.80 Å, the B —O distance 1.46 Å. The structure looks at first sight improbable because of the inherent strain and steric problems associated with a four-membered ring; the preferred tetrahedral geometry of the B and Si atoms is distorted considerably to give O —B —O and O —Si —O angles of slightly less than 90° compared to the ideal value of 109.5°. However, the ring is stabilized by O($2p$) → Si($3d$) π-bonding, accounting for the planarity of the ring and the approximately 90° O —Si —O angle, since this geometry maximizes the orbital overlap for such a bonding scheme.

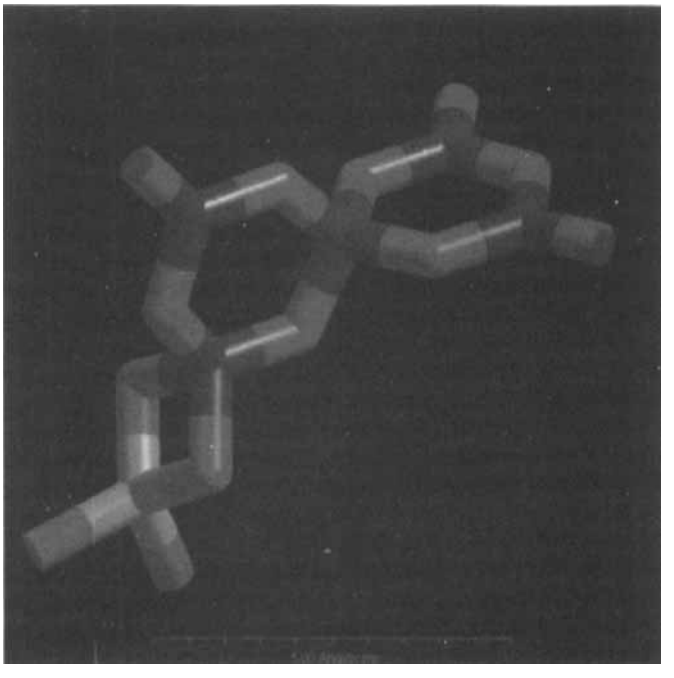

FIGURE 10 Energy minimised (AM1) conformation of the pentaborate plus silicate system. (See Color Plate VIII).

As in the previous molecular modelling study by Coveney and Humphries [3], the MNDO semi-empirical method was employed in MOPAC to optimise the conformation of this structure. However, an article published by its creator [24] states that a principal drawback to MNDO is that: "Four-membered rings are too stable". We therefore chose an alternative molecular orbital approximation scheme, AM1, which the same author states is a distinct improvement over MNDO [25]; it is claimed that the problems encountered with four-membered rings using MNDO have been resolved with this improved semi-empirical method. All further work was thus carried out using the AM1 Hamiltonian. We found that the 4-membered ring was still stable using AM1.

In contrast to the physical adsorption of borates on the surface described above, this chemical method of binding to the silicate chains explains why the monomeric form of borate, $B(OH)_4^-$, is able to block growth of the silicate chains: *any boron atom co-ordinated by oxygens can equally well form this four-membered ring* preventing further extension of the silicate chain. Figure 11 shows $B(OH)_4^-$ monomers bonding to the end of the silicate chains in tobermorite, inhibiting their continued propagation. As we have repeatedly emphasised, the mechanism applies to *any growing calcium silicate hydrate containing chains of silicates*; it is not specific to tobermorite. Thus such borates can also inhibit growth of jennite, which contains silicate chains as in tobermorite, and xonotlite, which contains sheets of rings of silicates as shown in Figure 4 as well as growing silicate chains within amorphous silicates.

We may also consider possible mechanisms for the other (pH-dependent) polymeric borate anions shown in Figure 5 to inhibit silicate chain growth. A 4-membered ring engenders a degree of scepticism due to its inherent strain and steric problems. In the case of the hydrated triborate (**B**) and tetraborate (**C**) species, we can envisage a method of attachment involving a chemically more attractive 6-membered ring, as shown in Figure 14. These structures were optimised using MOPAC (AM1), and the 6-membered borosilicate ring was found to be stable in each case – the conformations adopted are shown in Figures 15 and 16. For the hydrated tetraborate, the stable species is that shown in Figure 14; for the hydrated triborate, the boroxine ring cleaves in order to accommodate the borosilicate ring. The 6-membered ring can also be formed by any transient diborate species in solution (see Fig. 12), which is equivalent to the hydrated triborate attachment having lost its HBO_3^{2-} "tail".

Any theory proposed in this way must be consistent with experimental evidence. It is also possible to make predictions using this model which can

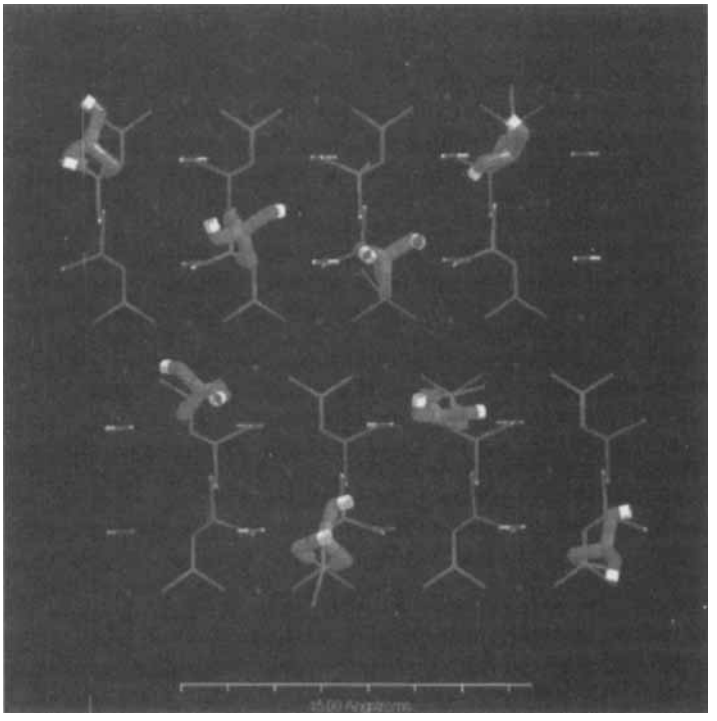

FIGURE 11 Inhibition of the growth of silicate chains in tobermorite by the monomeric borate unit. (See Color Plate IX).

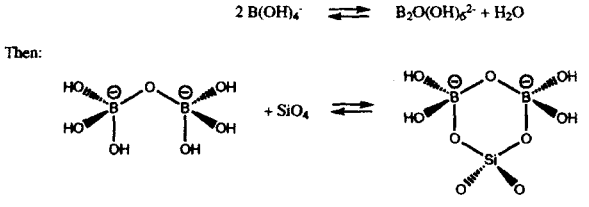

FIGURE 12 Transient diborate species may attach to a silicate via a six-membered ring.

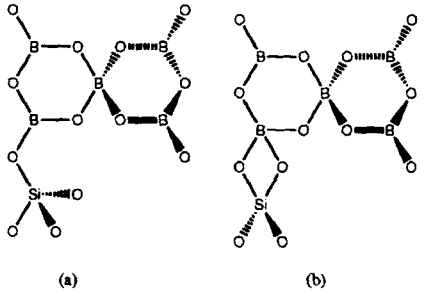

FIGURE 13 Two methods for the pentaborate anion to attach to a silicate chain.

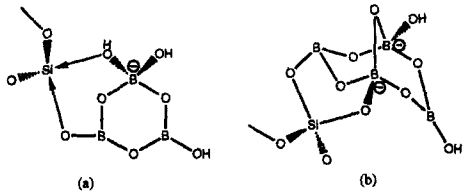

FIGURE 14 Hydrated triborate (a) and tetraborate (b) anions attaching to a silicate chain via a 6-membered ring.

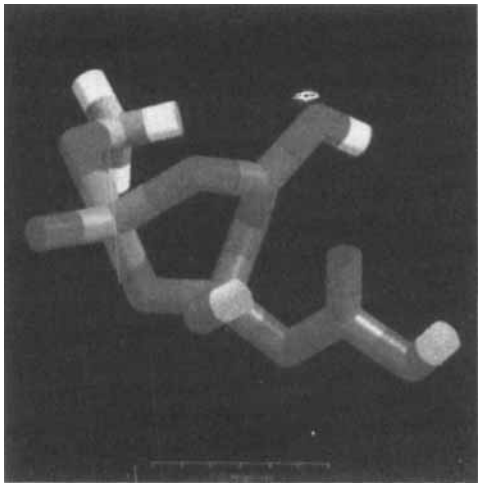

FIGURE 15 Energy minimised conformation of the hydrated triborate-plus-silicate system. (See Color Plate X).

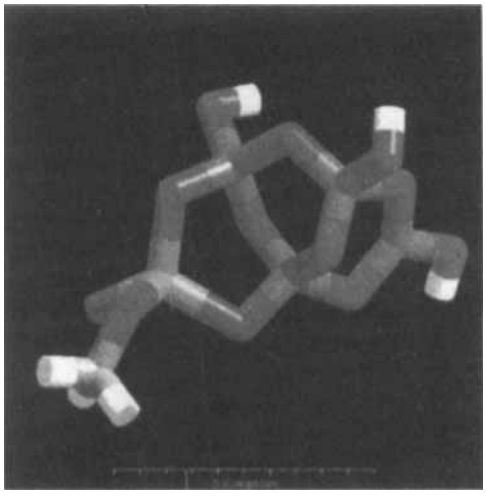

FIGURE 16 Energy minimised conformation of the hydrated tetraborate-plus-silicate system. (See Color Plate XI).

be tested experimentally. In particular, we used MOPAC to calculate observable vibrational frequencies. The CPU time needed to perform this calculation on the full pentaborate anion-plus-silicate chain system would have been prohibitive so instead a simplified model molecule was designed from which the vibrational frequencies characteristic of the four- and six-membered borosilicate rings could be determined. The four-membered ring model is shown in Figure 17(a), and consists of a tetrahedral borate group joined to a silicate group, with a methyl group in place of the silicate chain. The two borate oxygens attached to the ring have been protonated: this molecule therefore represents the situation when a $B(OH)_4^-$ unit bonds to the end of a chain. The presence of the methyl group is intended to model the geometry of the next Si atom in the chain; since we are only interested in the characteristic frequencies of the ring, this simplification is likely to be relatively unimportant. A similar model was used to elucidate the characteristic frequencies of the six-membered borosilicate ring, and is shown in Figure 17(b).

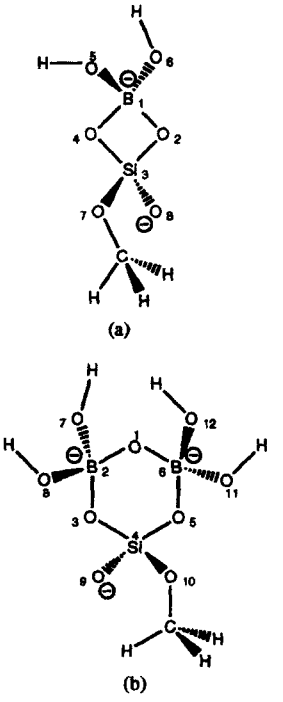

FIGURE 17 The model molecules used to study the vibrational frequencies characteristic of the borosilicate rings.

Using MOPAC, it is possible to analyse the vibrational modes calculated for the molecule shown in Figure 17(a) in order to determine which are characteristic of the four-membered ring. The molecule contains 14 atoms and thus has ($3 \times 14 - 6 =$) 36 vibrational modes. Of these, we considered only those in which (at least) the four most important contributions to the vibration resulted from the atoms of interest (i.e., discounting the hydrogen atoms and methyl group). In the mid infra-red spectrum (from 600 to 400 cm^{-1}), this gave the following eight vibrational frequencies:

$$688, 692, 803, 883, 957, 1077, 1090, 1167\,cm^{-1}$$

We repeated this calculation for the proposed six-membered borosilicate ring using the molecule shown in Figure 17(b), obtaining the following eleven vibrational frequencies:

$$718, 835, 843, 926, 993, 1014, 1058, 1079, 1095, 1112, 1158\ cm^{-1}$$

It is these frequencies which if observed experimentally would provide conclusive proof as to the validity of the mechanism proposed here. All of the vibrational frequencies given above should be observable in the infra-red spectrum since all the corresponding transitions have a non-zero transition dipole moment. The complete set of data calculated by MOPAC about these vibrations is given in Appendices A and B.

5. MOLECULAR DESIGN OF A NOVEL RETARDER

On the basis of our modelling work, which appears to provide a satisfactory explanation for the observed potency of the borate species currently in use, we are able to propose a novel high-temperature boronate retarder aid that we might expect to be even more effective than those used at present. As described above, our proposed mechanism of retardation is that borate species bond chemically to the end of silicate chains, inhibiting their further growth. It therefore seems likely that a borate species which can simultaneously inhibit the extension of more than one of the growing chains will be a more potent retarder. To this end, we attempted to design a molecule containing three borate groups; these were arranged in such a way that the distance between them was similar to the distance between silicate tetrahedra on the ($\bar{1}20$) surface of tobermorite.

The resulting macrocyclic triboronate anion (an oxo-aza 18-crown-6 derivative related to a phosphonate proposed in [3]) is shown in Figure 18.

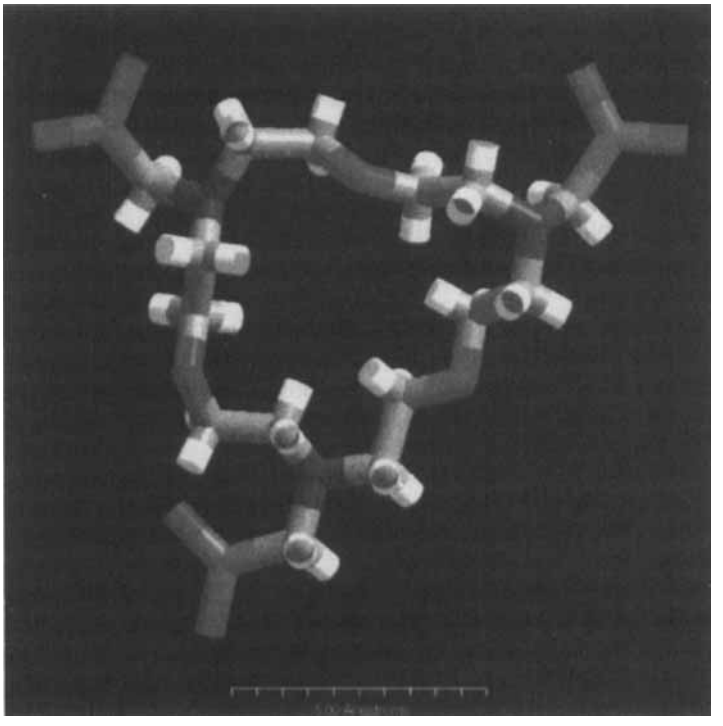

FIGURE 18 The oxo-aza 18-crown-6 macrocyclic boronate (C: grey, N: brown). (See Color Plate XII).

This anion is shown bonding to the ($\bar{1}20$) surface of tobermorite in Figure 19 according to the mechanisms which we proposed in Section 4.2, i.e., it is linked to the surface by three four-membered borosilicate rigns. If the $B(OH)_4^-$ monomer were also independently available in the slurry, we would anticipate that six-membered borosilicate rings would be likely to form instead. It can be seen from the figure that the geometry of this macrocyclic anion is such that the three borate groups can each bond to a surface silicate, inhibiting growth of *three* silicate chains in the tobermorite phase. For this reason, we would expect this molecule to be a powerful cement setting retarder.

We then investigated whether this molecule might also prove suitable for inhibiting the growth of xonotlite within the cement slurry. This requires a molecule of suitable geometry to prevent extension of the chains of silicate rings in the *b* direction. The surface perpendicular to this direction is the (010) plane, since xonotlite belongs to the orthorhombic crystal system, and this surface is shown in Figure 20. These geometric studies confirmed that

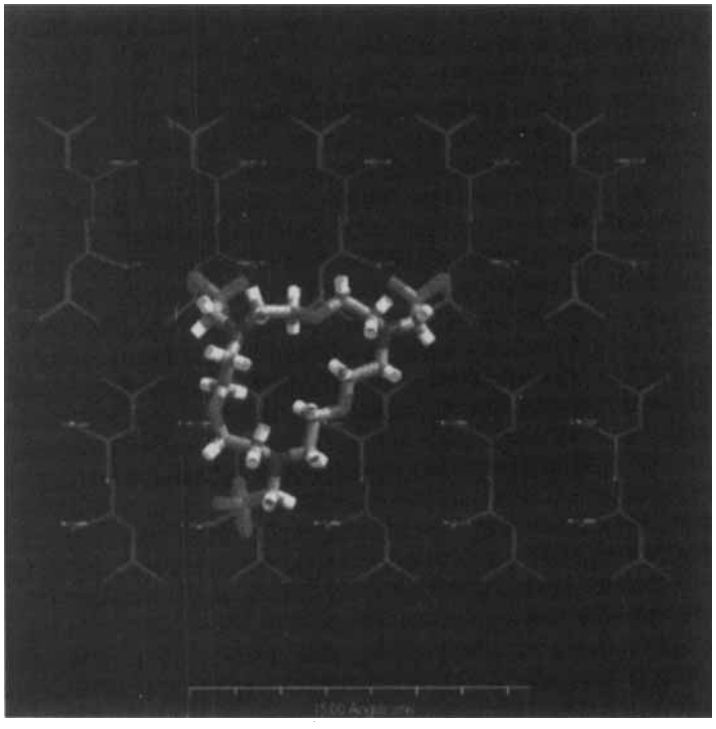

FIGURE 19 The energy minimised conformation of the oxo-azo crown macrocycle bonded to the ($\bar{1}20$) surface of tobermorite. (See Color Plate XIII).

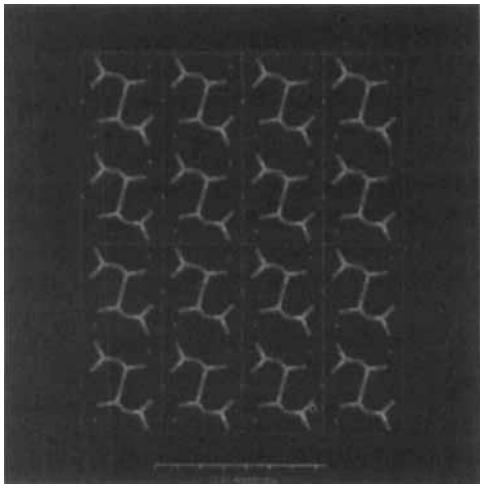

FIGURE 20 The (010) surface of xonotlite. (See Color Plate XIV).

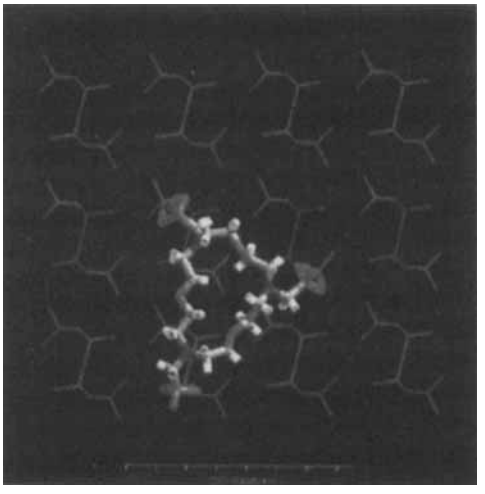

FIGURE 21 The energy minimised conformation of the oxo-aza crown macrocycle bonded to the (010) surface of xonotlite. (See Color Plate XV).

the same boronate anion as proposed above has the correct structure for bonding chemically to silicates on this surface; the energy minimised configuration adopted by our novel retarder on the (010) surface of xonotlite is shown in Figure 21.

The novel macrocyclic boronate which we have designed should, on the basis of our proposed mechanism, act as an effective cement retarder aid at high temperatures since it may inhibit growth of both tobermorite and xonotlite crystals within the cement slurry, as well as efficiently inhibiting propagating silicate chain growth within the amorphous phase. In addition, such a molecule might also display improved ambient temperature retardation since its geometry is such that it may also dock exactly into the (001) surface sulphate sites in ettringite, inhibiting its growth by the same mechanism as is described in [3]. As ever, the proof of the pudding is in the eating: we believe it will be possible to synthesize this molecule reasonably easily and thereafter its retarding properties can be investigated experimentally.

6. CONCLUSIONS

Using a range of computational techniques, we find that we are able to provide a plausible explanation for the effectiveness of borate retarders. This has proved possible because we started with a simple nonlinear chemical

kinetic model of the hydration process which isolates a small number of rate-determining steps [1, 9]. The one key step relevant to the molecular modelling task concerns the inhibition of growth of silicate chains during the hydration process.

We have been able to predict observable vibrational frequencies of the borosilicate complexes implicated and also to design a novel boronate retarder on the basis of our proposed mechanism of retardation; future experimental studies might be able to establish the validity of our proposals.

Acknowledgements

We are are grateful to Chris Hall, Andy Whiting, Will Humphries, Véronique Barlet and Michel Michaux for some helpful discussions at various stages during this work.

References

[1] Billingham, J. and Coveney, P. (1993). "Simple chemical clock reactions – Application to cement hydration", *J. Chem. Soc., Faraday Trans.*, **89**, 3021
[2] Taylor, H. F. W., *Cement Chemistry*, (Academic Press, 1989).
[3] Coveney, P. V. and Humphries, W. (1996). "Molecular modelling of the mechanism of action of phosphonate retarders on hydrating cements", *J. Chem. Soc., Faraday Trans.*, **92**, 831.
[4] Coveney, P. V., Davey, R. J., Griffin, J. L. W. and Whiting, A. (1997). "Controlling the setting of cement: molecular engineering of the world's most abundant construction material", preprint.
[5] Fujii, K. and Kondo, W. (1983). "Estimation of thermochemical data for calcium silicate hydrate (C —S —H)", *J. Am. Ceram. Soc.*, **66**, C220.
[6] Kantro, D. L., Brumauer, S. and Weise, C. H. (1962). "Development of surface in the hydration of calcium silicates. II. Extension of investigations to earlier and later stages of hydration", *J. Phys. Chem.*, **66**, 1804.
[7] Taylor, H. F. W. (1986). "Proposed structure for calcium silicate hydrate gel", *J. Am. Ceram. Soc.*, **69**, 464.
[8] Casey, W. H., Westrich, H. R., Banfield, J. F., Ferruzzi, G. and Arnold, G. W. (1993). "Leaching and reconstruction at the surfaces of dissolving chain-silicate minerals", *Nature*, **366**, 253.
[9] Wattis, J. A. D. and Coveney, P. V. (1997). "General nucleation theory with inhibition for chemically reacting systems", *J. Chem. Phys.*, **106**, 9122,
[10] Kalousek, G. L. and Chow, S. Y. (1976). Society of Petroleum Engineers paper.
[11] Hamid, S. A. (1981). "The crystal-structure of the 11-Å natural tobermorite $Ca_{2.25}[Si_8O_{7.5}(OH)_{1.5}]H_2O$" *Zeitschrift für Kristallographie*, **154**, 189.
[12] Most of our work was performed using the molecular modelling package CERIUS^2, Molecular Simulations Inc. (1994).
[13] Bravais, A., Études Crystallographiques (Paris, 1913).
[14] Friedel, G. (1907). *Bull. Soc. Fr. Mineral*, **30**, 326.
[15] Donnay, J. D. H. and Harker, D. (1937). *Am. Mineral*, **22**, 463.
[16] Michaux, M., private communication with the authors.
[17] Bensted, J., Callaghan, I. C. and Lepre, A. (1991). "Comparative-study of the efficiency of various borate compounds as set-retarders of Class G oilwell cement" *Cement and Concrete Research*, **21**, 663.

[18] Edwards, J. O. and Ross, V. F. (1967). "The chemistry of boron and its compounds" Ch.3, Ed. E. L. Muetterties (Wiley, New York).
[19] Stewart, J. J. P., MOPAC Version 6.0, QCPE No. 455 (Department of Chemistry, Indiana University, 1990).
[20] Rappé, A. K., Casewit, C. J., Colwell, K. S., Goddard, W. A. and Skiff, W. M. (1992). "UFF, a full periodic-table force-field for molecular mechanics and molecular-dynamics simulations", *J. Am. Chem. Soc.*, **114**, 10024.
[21] Rappé, A. K. and Goddard, W. A. (1991). "Charge equilibration for molecular-dynamics simulations", *J. Phys. Chem.*, **95**, 3358.
[22] Andersen, H. C. (1980). *J. Chem. Phys.*, **72**, 2384.
[23] Parrinello, M. and Rahman, A. (1981). "Polymorphic transitions in single-crystals-a new molecular-dynamics method", *J. Appl. Phys.*, **52**, 7182.
[24] Stewart, J. J. P. (1990). "Special issue – MOPAC – A new semiempirical molecular-orbital program", *J. Computer-Aided Mol. Design*, **4**, 1.
[25] Stewart, J. J. P., *Reviews in Computational Chemistry*, Eds. K. B. Lipkowitz and D. B. Boyd (VCH, 1990).
[26] Stewart, J. J. P., *MOPAC Manual (Sixth Edition)* (October, 1990).

APPENDIX A. VIBRATIONAL MODES OF THE FOUR-MEMBERED BOROSILICATE RING

The abbreviations used are as follows:

Frequency is the frequency of the vibration in wavenumbers (cm^{-1}).

T-Dipole is the transition dipole moment.

Travel and Red. mass are respectively the idealized distance travelled and the reduced mass which represent the assumed simple harmonic motion of the vibration. The reduced mass is assumed to be attached by a spring to an infinite mass. Its displacement is the "travel" variable.

The third column is a list of all pairs of atoms that contribute significantly to the energy of the mode; the atom-numbering systems used are shown in Figure 17. The percentage energy contribution of this pair to the mode is shown in the last column, calculated as described in [26].

TABLE

		Atom Pair	*Energy Contribution*
Vibration 16			
Frequency	687.87	Si 3–O 2	17.2%
T-Dipole	2.5216	Si 3–O 7	15.1%
Travel	0.0721	B 1–O 2	12.9%
Red. mass	9.4211	Si 3–O 4	11.9%
Vibration 17			
Frequency	691.91	Si 3–O 7	18.3%
T-Dipole	2.6865	Si 3–O 4	15.7%
Travel	0.0715	B 1–O 4	11.8%
Red. mass	9.5449	Si 3–O 2	9.2%
Vibration 18			
Frequency	803.25	Si 3–O 2	17.7%
T-Dipole	3.9231	Si 3–O 4	15.6%

TABLE (Continued)

Travel	0.0684	B 1–O 2	10.9%
Red. mass	8.9642	B 1–O 4	9.5%
Vibration 19			
Frequency	882.83	Si 3–O 4	19.8%
T-Dipole	2.2552	B 1–O 4	18.2%
Travel	0.0683	Si 3–O 2	17.7%
Red. mass	8.1929	B 1–O 2	14.5%
Vibration 20			
Frequency	956.80	B 1–O 2	22.0%
T-Dipole	2.7220	B 1–O 4	20.4%
Travel	0.0742	B 1–Si 3	14.4%
Red. mass	6.4057	B 1–O 6	12.8%
		B1–O 5	12.5%
Vibration 21			
Frequency	1077.36	B 1–O 6	20.2%
T-Dipole	5.9817	B 1–O 5	14.3%
Travel	0.0653	B 1–Si 3	14.3%
Red.mass	7.3448	B 1–O 4	13.8%
		B 1–O 2	13.7%
Vibration 22			
Frequency	1089.51	B 1–O 5	19.7%
T-Dipole	3.9999	B 1–Si 3	13.3%
Travel	0.0673	B 1–O 2	13.1%
Red. mass	6.8362	B 1–O 4	12.1%
		B 1–O 6	12.1%
Vibration 23			
Frequency	1167.26	B 1–Si 3	16.0%
T-Dipole	1.5181	Si 3–O 8	12.6%
Travel	0.0620	B 1–O 2	11.3%
Red. mass	7.5216	B 1–O 4	11.2%
		B 1–O 6	11.1%
		B 1–O 5	10.5%

APPENDIX B. VIBRATIONAL MODES OF THE SIX-MEMBERED BOROSILICATE RING

		Atom Pair	*Energy Contribution*
Vibration 27			
Frequency	717.55	Si 4–O 3	13.4%
T-Dipole	1.3940	Si 4–O 5	13.2%
Travel	0.0754	B 6–O 5	11.6%
Red. mass	8.2628	B 2–O 3	11.3%
		B 2–O 1	11.3%
		B 6–O 1	11.0%
Vibration 28			
Frequency	835.00	Si 4–O 3	12.2%
T-Dipole	3.7639	B 2–O 1	8.8%
Travel	0.0682	B 2–O 3	8.0%
Red. mass	8.6732	B 6–O 11	7.6%

TABLE (Continued)

Vibration 29			
Frequency	842.65	Si 4–O 5	12.3%
T-Dipole	1.9297	B 6–O 5	10.4%
Travel	0.0706	B 2–O 8	9.7%
Red. mass	8.0185	B 6–O 1	9.0%
Vibration 30			
Frequency	926.43	Si 4–O 5	14.6%
T-Dipole	0.2214	Si 4–O 3	14.0%
Travel	0.0648	B 2–O 3	8.8%
Red. mass	8.6674	B 6–O 5	8.3%
Vibration 31			
Frequency	993.00	B 2–O 7	15.6%
T-Dipole	2.6904	B 2–O 8	13.5%
Travel	0.0744	B 2–O 1	12.0%
Red. mass	6.1270	B 2–O 3	11.5%
		B 2–Si 5	11.2%
Vibration 32			
Frequency	1014.10	B 6–O 12	17.7%
T-Dipole	2.6921	B 6–O 11	12.5%
Travel	0.0746	B 6–O 5	12.5%
Red. mass	5.9747	B 6–Si 4	11.7%
		B 6–O 1	11.6%
Vibration 33			
Frequency	1058.41	B 6–O 5	19.6%
T-Dipole	2.0836	B 6–O 11	14.3%
Travel	0.0735	B 6–Si 4	12.2%
Red. mass	5.8949	B 6–O 1	12.1%
		B 6–O 12	11.7%
Vibration 34			
Frequency	1078.67	Si 4–O 9	28.4%
T-Dipole	6.6113	Si 4–O 5	10.9%
Travel	0.0557	Si 4–O 3	10.6%
Red. mass	10.0804	Si 4–B 6	9.7%
Vibration 35			
Frequency	1094.69	B 2–O 1	21.0%
T-Dipole	4.5899	B 6–O 1	16.1%
Travel	0.0694	B 2–O 8	9.6%
Red. mass	6.3853	B 2–O 7	8.4%
Vibration 36			
Frequency	1112.43	B 2–O 8	11.4%
T-Dipole	2.1465	B 2–O 3	11.1%
Travel	0.0728	B 6–O 1	10.2%
Red. mass	5.7193	B 2–O 1	10.0%
Vibration 37			
Frequency	1158.19	B 2–O 3	19.0%
T-Dipole	4.1435	B 2–O 1	10.2%
Travel	0.0738	B 2–O 7	9.3%
Red. mass	5.3381	B 2–O 8	9.0%